IOPscience iopscience.iop.org

Home Search Collections Journals About Contact us My IOPscience

Magnetic properties of $Nd_{1-x}Ag_xMnO_3$ compounds

This article has been downloaded from IOPscience. Please scroll down to see the full text article.

2008 J. Phys.: Condens. Matter 20 505212

(http://iopscience.iop.org/0953-8984/20/50/505212)

View the table of contents for this issue, or go to the journal homepage for more

Download details:
IP Address: 129.252.86.83
The article was downloaded on 29/05/2010 at 16:50

Please note that terms and conditions apply.

J. Phys.: Condens. Matter **20** (2008) 505212 (8pp) doi:10.1088/0953-8984/20/50/505212

Magnetic properties of $Nd_{1-x}Ag_xMnO_3$ compounds

S K Srivastava and S Ravi

Department of Physics, Indian Institute of Technology Guwahati, Guwahati 781039, India

E-mail: sravi@iitg.ernet.in

Received 10 June 2008, in final form 6 October 2008
Published 12 November 2008
Online at stacks.iop.org/JPhysCM/20/505212

Abstract

Polycrystalline $Nd_{1-x}Ag_xMnO_3$ compounds were prepared in single-phase form up to 20% of Ag doping. They are found to crystallize in the *Pbnm* space group with an increase in lattice parameters with doping. The magnetic properties were studied by measuring dc magnetization and ac susceptibility. A paramagnetic to ferromagnetic transition along with the signature of the presence of competing antiferromagnetic interaction has been observed. The saturation magnetic moment up to 2.2 μ_B per formula unit has been observed at 78 K. The measured magnetization has been analyzed by using the Brillouin function and by taking into account the ferromagnetic interaction. The measured magnetization has been explained on the basis of spin canting with a ferromagnetic component along a unique axis and with an antiferromagnetic interaction in a plane perpendicular to the axis. The average magnetic moment estimated from the Curie–Weiss law fit in the paramagnetic region is comparable to the theoretical magnetic moment due to Mn^{3+}/Mn^{4+} and Nd^{3+} ions. The analyses of frequency variation of ac susceptibility and harmonic susceptibility indicate the presence of spin-glass-like behavior below the ferromagnetic transition temperature.

(Some figures in this article are in colour only in the electronic version)

1. Introduction

$La_{1-x}A_xMnO_3$ (A = alkaline earth)-based colossal magnetoresistivity (CMR) materials are widely studied compared to other rare-earth-based CMR materials [1–6]. The $La_{1-x}A_xMnO_3$ series is found to have a large e_g electron bandwidth due to its large A site ionic size and hence strong double exchange (DE) ferromagnetic (FM) interaction [1–6] with higher transition temperature. On the other hand, the Nd–Mn–O series falls in the category of medium-size e_g bandwidth and hence the ionic size of doped materials plays a very sensitive and crucial role in tuning the magnetic properties in this system. Troyanchuk *et al* [7] studied systematically the magnetic properties of $Nd_{1-x}Ca_xMnO_3$ compounds and observed ferromagnetic (FM) transition with T_c around 110 K followed by a broad peak at around 72 K. The maximum saturation magnetization was found to be 2.8 μ_B at 5 K for a 1 T field. A large difference between zero-field-cooled (ZFC) and field-cooled (FC) magnetization was observed with electrical resistivity following semiconducting behavior. Liu *et al* [8] prepared the $Nd_{1-x}Ca_xMnO_3$ compounds for $x = 0$–1 and found that all the materials exhibited semiconducting behavior with the magnetic properties demonstrated by charge ordering and antiferromagnetic (AFM) transition. However, the application of magnetic field was found to induce semiconductor–metal and AFM–FM transition in the composition range $0.30 \leqslant x \leqslant 0.45$. The charge ordering and its destruction by the application of a large magnetic field were reported by Tokunaga *et al* [9] in $Nd_{0.5}Ca_{0.5}MnO_3$. Rao *et al* [10] demonstrated the destruction of charge ordering and the introduction of an FM transition by preparing the material in nanophase form. In the $Nd_{0.7}Sr_{0.3}MnO_3$ series, FM and metal–insulator (M–I) transitions have been observed with T_c in the range of 230–250 K because of its relatively large A site ionic size ($\langle r_A \rangle = 1.212$) compared to the (Nd, Ca)–Mn–O series [11–13]. However, in half-doped $Nd_{0.5}Sr_{0.5}MnO_3$ material charge ordering has been reported at around 150 K from detailed neutron diffraction, magnetization and electrical resistivity studies [14–18]. In the $Nd_{1-x}Ba_xMnO_3$ series, even though the $\langle r_A \rangle$ value is quite large, FM was observed in a narrow composition range of $x = 0.2$–0.4 with a relatively lower transition temperature of 120 K and with electrical resistivity of the order of kΩ cm [19, 20]. Thus the double exchange (DE) interaction is not purely driven by the $\langle r_A \rangle$

 © 2008 IOP Publishing Ltd Printed in the UK

size or e_g electron bandwidth. There are a few reports on single-crystal samples of $Nd_{0.7}Pb_{0.3}MnO_3$, where FM and M–I transitions have been observed at around 150 K [21–23]. It was also predicted that, in these materials, Nd ions order antiferromagnetically with spin canting. Recently the monovalent alkali-ion-doped, $Nd_{1-x}Na_xMnO_3$ series was studied by a few groups for $x = 0.1$–0.25 and found that these materials exhibit charge ordering at around 180 K followed by a weak FM transition at 110 K [24–26]. The electrical resistivity follows semiconducting behavior without any metal–insulator transition. However, a metal–insulator transition could be induced by the application of a magnetic field of the order of 3 T [26].

Even though there are several reports on divalent alkaline-earth-doped Nd–Mn–O series, the work on monovalent doping in place of Nd is limited. The monovalent doping has some advantages over divalent doping. Each doped monovalent atom oxidizes two Mn ions from the Mn^{3+} to the Mn^{4+} state. Thus, the optimum ratio of Mn^{3+} and Mn^{4+} ions can be obtained by doping a relatively small fraction of monovalent atoms and hence with minimum lattice distortion. The Ag doping in the $La_{1-x}Ag_xMnO_3$ series has been found to be quite successful in achieving CMR behavior in the vicinity of room temperature [27–30]. Moreover, the ionic size of Ag^{1+} is greater than some of the alkaline earth and alkali ions, so in the present work, we have prepared $Nd_{1-x}Ag_xMnO_3$ compounds for $x = 0.05$–0.20. We have studied their magnetic properties by measuring dc magnetization and ac susceptibility. These materials are found to exhibit ferromagnetic insulating behavior along with competing magnetic interaction. The detailed study of frequency variations of ac susceptibility and third harmonic susceptibility leads to the conclusion of the presence of spin-glass-like behavior.

2. Experimental details

Polycrystalline samples of $Nd_{1-x}Ag_xMnO_3$ ($x = 0.05$, 0.10, 0.15, 0.20) were prepared by the conventional solid state reaction method. A stoichiometric ratio of Nd_2O_3, $AgNO_3$ and manganese acetate with 99.9% purity were weighed and mixed thoroughly under acetone. The mixture was presintered at 1000 °C for 40 h in a step-by-step process by heat treating at a few intermediate temperatures. The final sintering in pellet form was carried at 1150 °C for 40 h. X-ray diffraction patterns (XRD) were recorded by using a Bruker D8 Advance XRD machine with Cu Kα radiation. Recording of the microstructure image and compositional analysis have been carried out by using a LEO scanning electron microscope (SEM) equipped with an Oxford energy-dispersive spectrometer (EDS).

The temperature variations of zero-field-cooled (ZFC) and field-cooled (FC) magnetization (M) were measured by using a Lakeshore model no. 7410 vibrating sample magnetometer under 20 mT magnetic field (B) from 80 to 350 K. The magnetization loop was measured by varying B up to 2 T. Temperature variation of linear ac susceptibility (χ_1', χ_1'') was measured by the mutual inductance bridge method for an ac field amplitude of 0.6 mT operated at a frequency $f =$ 333 Hz. The frequency variation of linear ac susceptibility measurements was carried out at four different frequencies, namely 333, 1333, 3333 and 6333 Hz and for an applied field of 0.2 mT. The third harmonic susceptibility (χ_3', χ_3'') versus temperature was measured for an ac field amplitude of 0.2 mT. The third harmonic susceptibility signal was measured using a dual-phase lock-in-amplifier by setting the reference frequency as $3f$. The oxidation state of Mn was determined by a chemical titration method, in which the samples were dissolved in dilute sulfuric and phosphoric acids with an addition of an excess amount of $Fe(NH_4)_2(SO_4)_2$ and were titrated against self-indicating $KMnO_4$ solution.

Table 1. Parameters obtained from the Rietveld analysis of XRD patterns for samples $Nd_{1-x}Ag_xMnO_3$ ($x = 0.05$, 0.10, 0.15, 0.20). Errors in lattice parameters and unit cell volume are shown in brackets.

Sample/parameter	$x = 0.05$	$x = 0.10$	$x = 0.15$	$x = 0.20$
Space group	*Pbnm*	*Pbnm*	*Pbnm*	*Pbnm*
$a = b$ (Å)	5.4091 (0.0016)	5.4271 (0.0018)	5.4292 (0.0016)	5.4205 (0.0015)
b (Å)	5.6276 (0.0019)	5.5296 (0.0020)	5.5252 (0.0018)	5.5638 (0.0017)
c (Å)	7.6045 (0.0024)	7.6675 (0.0028)	7.6728 (0.0026)	7.6344 (0.0024)
Volume (Å)	231.5 (0.1)	230.1 (0.1)	230.2 (0.1)	230.2 (0.1)
χ^2 (%)	1.56	2.59	2.64	2.53
R_p (%)	3.14	5.75	5.33	4.24
R_f (%)	10.6	13.0	8.85	8.54
R_{Bragg} (%)	12.4	14.6	11.1	9.67
$\langle Mn–O_1 \rangle$ (Å)	2.0090	1.9909	2.0118	2.0240
$\langle Mn–O_2 \rangle$ (Å)	2.0072	1.9672	1.9807	1.9904
$Mn–O_1–Mn$ (deg)	142.3	148.7	144.9	141.1
$Mn–O_2–Mn$ (deg)	152.9	159.8	155.7	154.6
$\langle r_A \rangle$ (Å)	1.169	1.175	1.180	1.186
Tolerance factor (t)	0.864	0.892	0.879	0.874
Mn valence	3.14	3.25	3.32	3.38

3. Results and discussions

The $Nd_{1-x}Ag_xMnO_3$ compounds for $x = 0.05$, 0.10, 0.15 and 0.20 are found to be in single-phase form as per the XRD pattern. These XRD patterns were analyzed with the help of the fullprof program by the Rietveld refinement technique [31] and they could be refined as per the *Pbnm* space group. A typical XRD pattern along with Rietveld refinement is shown in figure 1 for $x = 0.15$. The refined lattice parameters and unit cell volume are listed in table 1. The lattice parameters a and c are found to increase with doping up to $x = 0.15$ due to the replacement of the Nd^{3+} ion by larger Ag^{1+} ions. However, the lattice parameter b is found to decrease with the increase in doping. As a result of elongation of MnO_6 octahedra along the a and c directions, there is a counter effect of contraction along the b direction. Such behavior has been observed by Tang *et al* [26] in the $Nd_{1-x}Na_xMnO_3$ series and the lattice parameters are found to be comparable to those of $Nd_{1-x}Na_xMnO_3$ compounds [26].

The Mn–O bond lengths and ∠Mn–O–Mn bond angles are calculated from the refined atomic positions and lattice

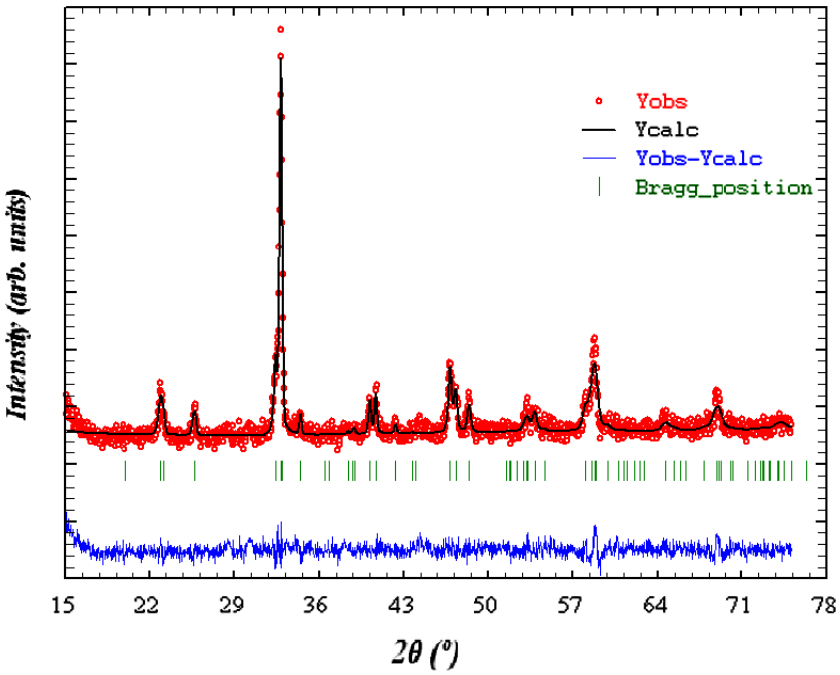

Figure 1. XRD pattern for the sample $x = 0.15$. The circles represent experimental points and the solid line represents Rietveld refined data. The bottom line shows the difference between experimental and refined data. The marked 2θ positions are the allowed Bragg peaks.

parameters and these values are listed in table 1. The Mn–O–Mn bond angle for $x = 0.10$ is found to be highest followed by the $x = 0.05$ sample. The microstructure morphology of the samples are found to be uniform with average particle size of the order of 2 μm. The chemical compositions determined from EDS analysis are found to be comparable to the nominal starting composition. The typical cationic ratio for the $x = 0.15$ sample is found to be Nd:Ag:Mn = 0.86:0.13:1.01. The average valence of Mn ions determined from chemical titration is given in table 1. The systematic increase in Mn valence with Ag doping depicts the formation of an Mn^{3+}/Mn^{4+} mixture with increase in Mn^{4+} concentration. The Goldschmidt tolerance factor, $t = (d_{Nd-O})/\sqrt{2}(d_{Mn-O})$ is found to vary from 0.86 to 0.89 with a maximum value for the $x = 0.10$ sample and they are given in table 1.

The temperature variations of magnetization for $x = 0.05$, 0.10, 0.15 and 0.20 samples in zero-field-cooled (ZFC) and field-cooled (FC) conditions are shown in figure 2. A sharp rise in magnetization at ~80 K has been observed for $x = 0.05$ and the complete transition could not be seen because of the low temperature limitation in the present set-up. The above transition temperature is comparable to the transition observed in the parent compound, $NdMnO_3$, reported in the literature [32, 33]. On the other hand, for doping concentrations $x \geqslant 0.10$, FM transitions are observed with T_c around 120 K. For $x = 0.10$ and 0.15, the T_c values are comparable and there is a clear bifurcation of ZFC and FC curves and such behavior could not be seen for the $x = 0.2$ sample because of the slightly lower transition temperature. The FM T_c observed in the present series is comparable to that reported for the $Nd_{1-x}Na_xMnO_3$ series [24–26]. However, unlike the (Nd, Na)–Mn–O series, we have not observed any charge ordering type of transitions.

The dc susceptibility χ_{dc} in the paramagnetic region was analyzed by using the Curie–Weiss law. The Curie temperature (θ_C) for all four samples was found to be positive and indicates the FM interaction. Thus the Ag doping gives rise to the generation of an Mn^{3+}/Mn^{4+} mixture and the Zener double exchange FM interaction. Typical plots of $1/\chi_{dc}$ versus temperature for $x = 0.10$ and 0.15 samples are shown in figure 3 along with Curie–Weiss law fitting. The FM transition temperature obtained from the M versus T curve and θ_C are given in table 2. The difference between T_C and θ_C are mainly due to the observed broad magnetic transition. The effective magnetic moment, μ_{eff}, was determined from the fitted Curie constant C and is given in table 2. It is found to decrease systematically with increase in Ag doping as a result of the oxidation of some of the Mn^{3+} ions into the Mn^{4+} state. The above μ_{eff} values obtained from the analysis of experimental data can be compared with the theoretical effective magnetic moment μ_{th}. By taking into account the magnetic moment contribution from Nd^{3+}, Mn^{3+} and Mn^{4+} ions, μ_{th} can be calculated as

$$\mu_{th}^2 = x_1\mu_1^2 + x_2\mu_2^2 + x_3\mu_3^2. \quad (1)$$

Here, x_1, x_2 and x_3 are the fractional concentrations of Nd^{3+}, Mn^{3+} and Mn^{4+} ions per formula unit. μ_1, μ_2, μ_3 are the theoretical magnetic moments of Nd^{3+}, Mn^{3+} and Mn^{4+} ions and their values due to the spin-only contribution are 3.62 μ_B, 4.9 μ_B and 3.87 μ_B, respectively. The μ_{th} values are tabulated in table 2 and they are comparable to μ_{eff} values and the minor difference between them is mainly due to error in the estimation of the concentration of Mn^{3+} and Mn^{4+} ions.

The magnetization loops measured at 78 K for $B = \pm 2$ T are shown in figure 4. There is a large increase in

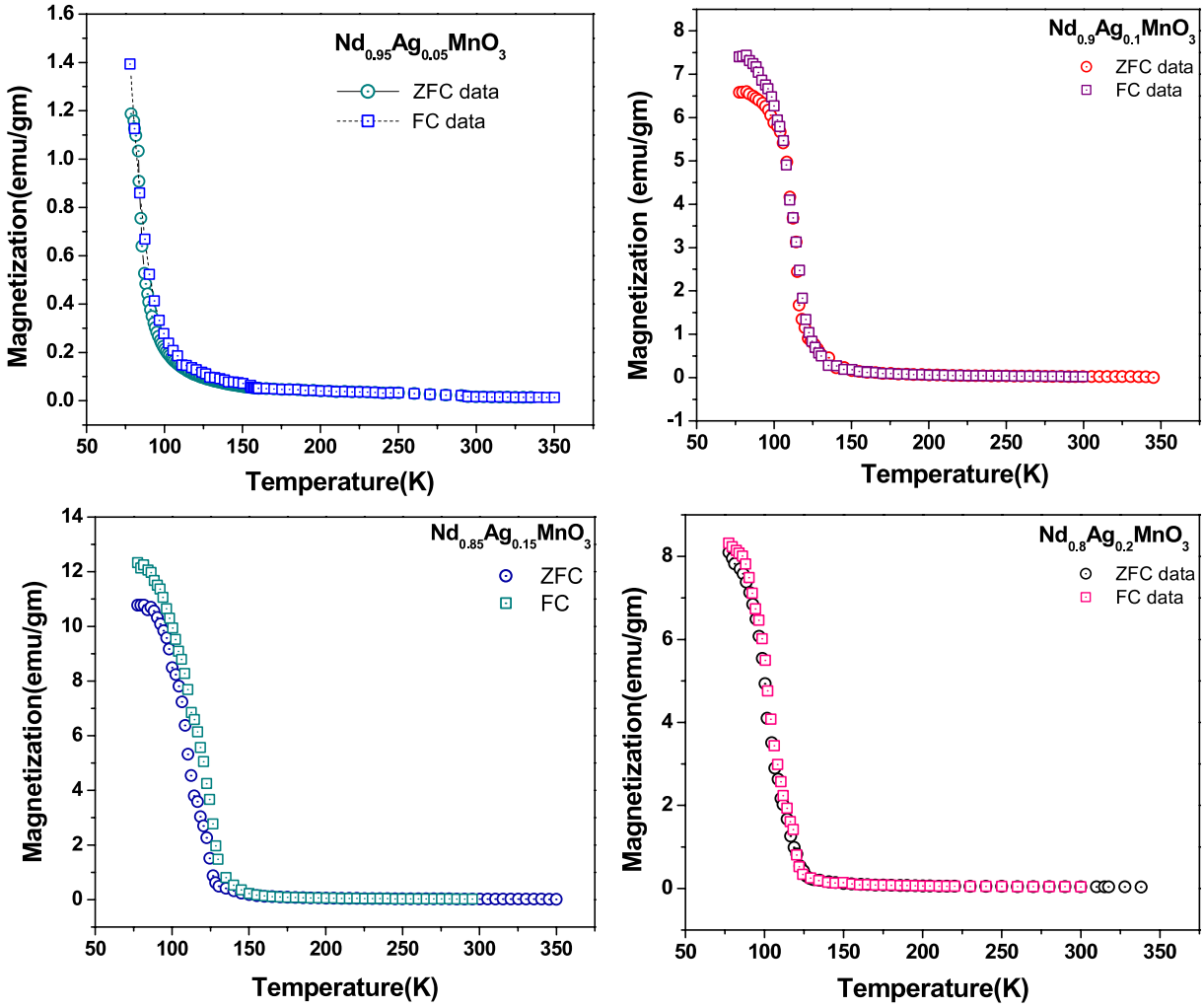

Figure 2. The temperature variation of (ZFC) zero-field-cooled (circles) and (FC) field-cooled (squares) magnetization curves for $x = 0.05$, 0.10, 0.15 and 0.20 samples.

Table 2. Parameters obtained from magnetic measurements. T_C is the ferromagnetic transition temperature. θ_C (Curie temperature) and μ_{eff} have been found from inverse dc susceptibility fitting. M_S and S_{eff} are the saturated magnetic moment and effective magnetic spin, respectively. τ_0 is the characteristic time constant calculated from frequency variation of ac susceptibility.

	Sample			
Parameter	$x = 0.05$	$x = 0.10$	$x = 0.15$	$x = 0.20$
T_C (K)	84.0	114.0	113.0	102.0
θ_C (K)	74.6	135.3	129.4	114.6
μ_{eff} (μ_B)	6.30	6.06	5.95	5.81
μ_{th} (μ_B)	5.96	5.83	5.69	5.60
M_S (μ_B/f.u.) at 78 K	0.34	1.98	1.85	1.31
S_{eff}	—	1.4 ± 0.1	1.8 ± 0.2	1.4 ± 0.1
$\tau_{0(10^{-8}\ s)}$	—	6.2	37.1	—
$z\nu$	—	1.33	0.90	—

saturation magnetization (M_S) as the doping concentration increases from 5% to 10%. The M_S value for $x = 0.10$ and 0.15 are comparable and it decreases for the $x = 0.20$ sample. The M_S value for the $x = 0.10$ and 0.15 samples are found to be relatively large compared to other samples. This can be understood on the basis of Mn^{3+}/Mn^{4+} concentrations, which are close to the optimum value of 0.7/0.3, where a relatively strong double exchange ferromagnetic interaction is observed in manganites. For the $x = 0.05$ sample, even though there is a minor ferromagnetic contribution, the magnetization is found to increase almost linearly with increase in magnetic field and it indicates the presence of a considerable AFM/paramagnetic contribution. The M_s value after subtracting the linear contribution is found to be 0.34 μ_B per formula unit. Even though the magnetization of higher doped materials has increased appreciably, their magnetization is less than the expected spin-only contribution of Mn ions. The M_S values after subtracting the linear contribution are given in table 2 for all the samples. The lack of hysteresis loss indicates the soft magnetic properties of the materials. By following the neutron diffraction results of Yu *et al* [32] and Munoz *et al* [33] in the $NdMnO_3$ parent compound and by assuming the canting of magnetic spins of Mn ions with its FM component parallel to the c axis and AFM component within the ab plane, the canting angle β with respect to the c axis can be estimated by determining the effective magnetic

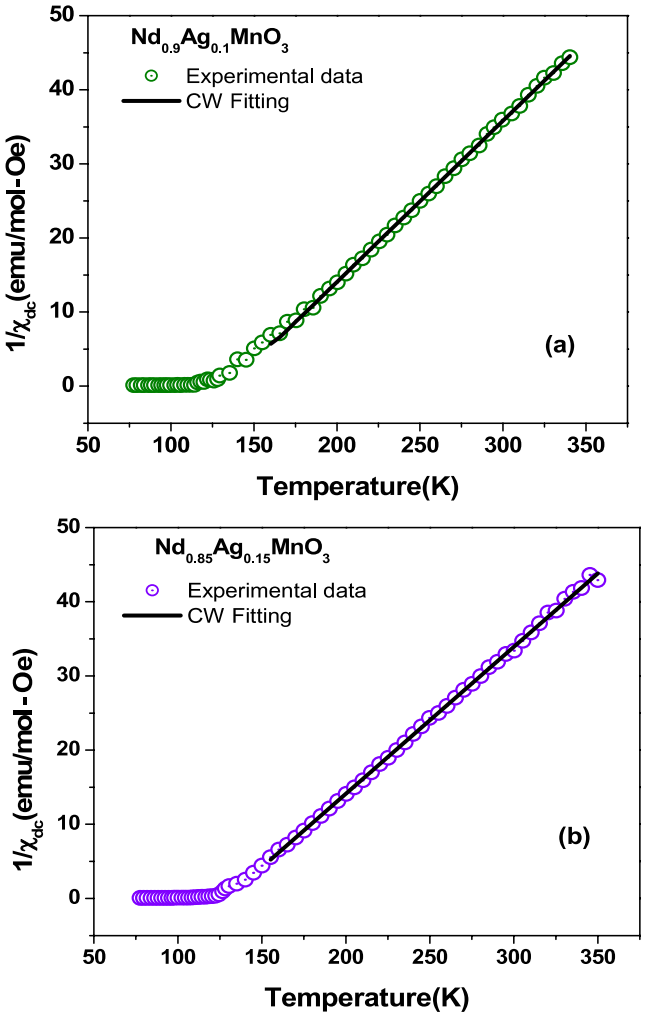

Figure 3. $1/\chi_{dc}$ versus temperature for the samples (a) $Nd_{0.90}Ag_{0.10}MnO_3$ and (b) $Nd_{0.85}Ag_{0.15}MnO_3$. Solid lines represent the fit to the Curie–Weiss law.

spin S_{eff}, which contributes to the ferromagnetic interaction. The field variation of magnetization after subtracting the linear contribution was fitted to the relation

$$M = M_0 B_S(x) \tag{2}$$

where

$$B_S(x) = \frac{1}{|S_{eff}|}\left[\left(S_{eff}+\frac{1}{2}\right)\coth x\left(S_{eff}+\frac{1}{2}\right) - \frac{1}{2}\coth\frac{x}{2}\right]. \tag{3}$$

Here, $M_0 = Ng\mu_B|S_{eff}|$, $x = \frac{g\mu_B}{kT}B$ and $B = B_a + \lambda M$. λ is the Weiss molecular field constant for ferromagnetic interaction and N is the number of atomic moments per unit volume. We have carried out the fit by assuming the λ values determined from the FM T_c and Curie constant C ($T_c = \lambda C/\mu_0$) for different samples. The typical magnetization fit for the $x = 0.10$ sample is shown in the inset of figure 4. We can see that the fitted data closely follow the experimental data. The fitted values of S_{eff} are given in table 2. The canting angle $\beta = \cos^{-1}(S_{eff}/S)$ has been calculated. Here S is the expected value of the spin for a particular sample corresponding to their

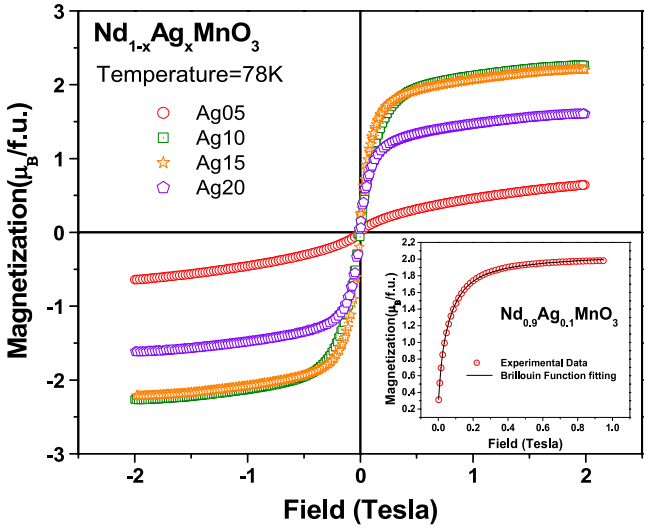

Figure 4. Magnetization versus magnetic field plots for $x = 0.05$, 0.10, 0.15 and 0.20 samples. The inset shows the Brillouin function fit to magnetization data (after subtracting the linear part) for the $x = 0.10$ sample.

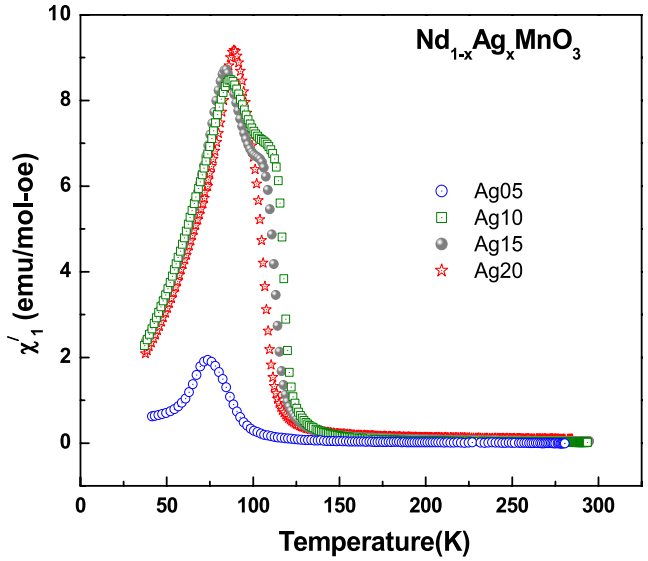

Figure 5. Temperature variation of linear ac susceptibility (χ_1') of $Nd_{1-x}Ag_xMnO_3$ ($x = 0.05$, 0.10, 0.15 and 0.20).

Mn valence. The typical values of β for $x = 0.10$ and 0.20 samples are found to be 42° and 40°, respectively. These values are comparable to the value reported for the $NdMnO_3$ compound [32].

The temperature variations of in-phase linear ac susceptibility (χ_1') are shown in figure 5 for $x = 0.05$, 0.10, 0.15 and 0.20 samples. A magnetic transition with peak effect has been observed for the $x = 0.05$ sample. It coincides with the transition observed from the magnetization measurement and AFM transition reported in the literature [33] for the parent $NdMnO_3$ compound. So, it is basically an FM transition with AFM component or vice versa due to spin canting. For further increase in doping concentration, i.e. $x \geqslant 0.10$, we can see the double exchange FM transition at around 115 K.

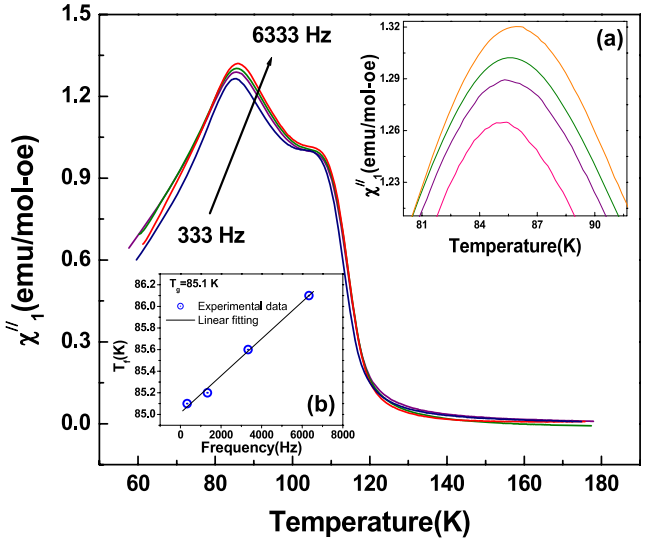

Figure 6. χ_1'' versus temperature (T) measured at frequencies $f = 333$, 1333, 3333 and 6333 Hz for the sample $Nd_{0.85}Ag_{0.15}MnO_3$. Inset (a) shows the magnified part of the low temperature peak and inset (b) shows the variation of freezing temperature with frequency.

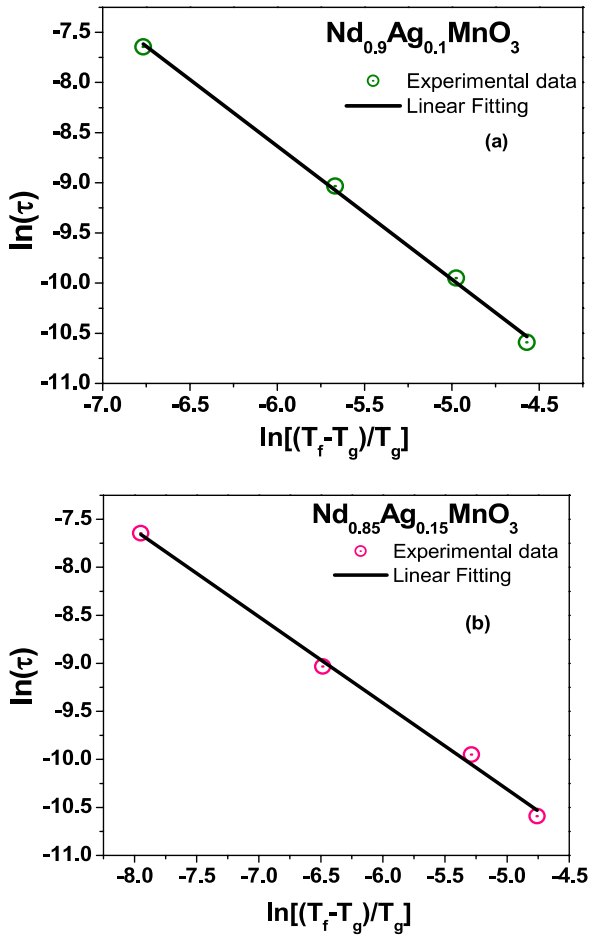

Figure 7. Plots of $\ln(\tau)$ versus $\ln[(T_f - T_g)/T_g]$ for (a) $Nd_{0.9}Ag_{0.1}MnO_3$ and (b) $Nd_{0.85}Ag_{0.15}MnO_3$ samples. Solid lines are fits based on equation (4).

In addition to that, a low temperature hump has also been observed and is comparable to the AFM transition observed in the $x = 0.05$ sample. The $1/\chi'$ versus T plots (not shown) for all the samples exhibit a linear behavior with positive Curie temperature. For $x = 0.2$ samples, FM T_c is found to reduce due to the increase in Mn^{4+} concentration beyond the optimum value and this transition merges with the low temperature hump. As the doping concentration increases, there are two effects, namely increase in concentration of Mn^{4+} ions and average A site ionic size. The increase in ionic size leads to the increase in ∠Mn–O–Mn bond angle. The increase in ∠Mn–O–Mn bond angle along with Mn^{3+}/Mn^{4+} pairs have a role in the strength of the double exchange ferromagnetic interaction. Thus, for a low level of doping, there is a dominant AFM interaction with weak FM due to spin canting. When the doping concentration is increased to 10 or 15%, appreciable FM has been observed. However, there is still a presence of AFM interaction due to spin canting. This is mainly due to the difficulty in getting the optimum Mn–O–Mn bond angle in the Nd series because of its low ionic size compared to the La series.

To further explore the magnetic behavior we have carried out the frequency variation of ac susceptibility. Typical plots of χ_1' versus temperature for the $x = 0.15$ sample are shown in figure 6 and they exhibit double peaks. The low temperature peak is found to shift towards higher temperature with increase in frequency as a result of spin-glass (SG)-like behavior. The low temperature peak is taken as the spin-glass freezing temperature T_f. The variation of T_f is shown in the inset of figure 6. Unlike the Mn-site-doped CMR materials [34–37], where a strong frequency dependence of T_f has been observed, we observe relatively weak frequency dependence. However, there is a clear shift in T_f, as can be seen from the inset of figure 6. The observed shift in T_f is comparable to that reported by Cao *et al* [38] in $(Nd, Sm)_{0.5}Ca_{0.05}MnO_3$ samples. Thus there is a weak spin-glass-like behavior in the present series. Similar behavior was found for the $x = 0.10$ sample. The dynamic property of spin glasses was analyzed based on a conventional power law model [39]:

$$\frac{\tau}{\tau_0} = \left[\frac{T_f - T_g}{T_g}\right]^{-Z\nu}. \tag{4}$$

Here, τ is the relaxation time corresponding to the measured frequency ($\tau = 1/f$), τ_0 is the spin flipping time and $z\nu$ is the critical exponent. T_g is the spin-glass transition temperature, which is equivalent to the freezing temperature in the limit of $\tau \to \infty$, i.e. $f \to 0$. The T_g values for $x = 0.10$ and 0.15 samples were determined by extrapolating the plots of T_f versus frequency to $f = 0$ and they are found to be 86.9 and 85.1 K, respectively. Plots of $\ln(\tau)$ versus $\ln[(T_f - T_g)/T_g]$ are shown in figure 7 for $x = 0.10$ and 0.15 samples. These data were fitted to equation (4) by varying the parameters τ_0 and $z\nu$ and the fitted data are shown as a solid line. The values of τ_0 and $z\nu$ are listed in table 2 for both samples. The values of τ_0 and $z\nu$ are comparable to those reported by Cao *et al* [38] in the $(Nd, Sm)_{0.5}Ca_{0.05}MnO_3$ system.

The values of T_g and $z\nu$ were independently determined by the following Kouvel–Fisher method [40]. According to

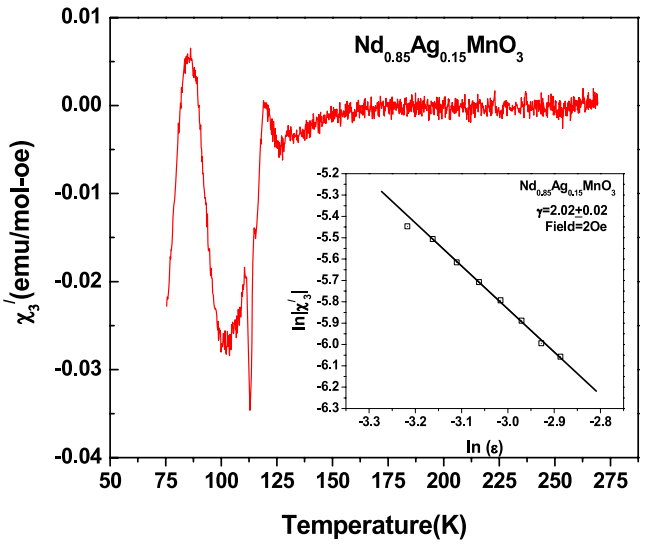

Figure 8. Third harmonic ac susceptibility (χ_3') versus T for the sample $Nd_{0.85}Ag_{0.15}MnO_3$. The inset shows the plot of ln $|\chi_3'|$ versus ln ε along with the fit to the scaling relation.

this technique, $\Lambda = [\frac{\mathrm{d}}{\mathrm{d}T}\ln(\frac{1}{\tau})^{-1} = \frac{T_\mathrm{f}}{z\upsilon \cdot T_\mathrm{g}} - \frac{1}{z\upsilon}$. Thus the plot of Λ versus T_f gives rise to T_g and $z\nu$. The values of T_g and $z\nu$ determined by this technique are found to be comparable to those obtained from the fit of equation (4). We also attempted to analyze the data in terms of the Vogel–Fulcher–Tamman exponential model [41] but the data could not be fitted to that model.

The observed frequency variation of fundamental harmonic susceptibility is not the unique property of spin-glass behavior. Another interesting magnetic property, i.e. superparamagnetism, also exhibits similar frequency variation of fundamental susceptibility. In order to ascertain unequivocally that the present low temperature transition is due to the spin-glass-like behavior, one has to carry out the measurement and analysis of harmonic susceptibility.

The typical plot of temperature variation of third harmonic ac susceptibility, χ_3', is shown in figure 8 for the $x = 0.15$ sample. It exhibits a sharp negative peak at 113 K and it coincides with the ferromagnetic transition temperature. In addition to that, there is a low temperature peak at 84 K. The position of the low temperature peak is closely comparable to that observed from the χ'' versus T plot (figure 6) and is attributed to the spin-glass transition temperature. It is comparable to the harmonic susceptibility of the ferromagnetic spin-glass material $Fe_{1.5}Mn_{1.5}Si$ reported by Chakravarti *et al* [42] and perovskite manganites [36, 37].

The unique property of spin-glass material is that their χ_3 values follow the critical scaling relation $\chi_3' \alpha \varepsilon^{-\gamma}$ [43]. Here, $\varepsilon = (T - T_\mathrm{g})/T_\mathrm{g}$ and γ is the critical exponent of the spin-glass transition. The plot of ln $|\chi_3'|$ versus ln(ε) is shown in the inset of figure 8 for the sample $x = 0.15$ and it exhibits a linear behavior. They were fitted to a linear equation by varying the parameter γ and the fitted data are shown as a solid line. The value of γ is found to be 2.02 ± 0.02 for the $x = 0.15$ sample. The present γ value is comparable to $\gamma = 2.3 \pm 0.2$, reported for the AgMn spin-glass system [44] and $\gamma = 2.2 \pm 0.2$ reported for PdMn spin glass material [45]. However, it differs considerably from the values reported for other spin-glass systems [39] and manganites [37, 46]. According to Mathieu *et al* [46], the critical exponent corresponding to the three-dimensional Heisenberg like model is 2.3 and the critical exponent of the present material can be compared to this model. Thus the low temperature transition observed in the linear and nonlinear ac susceptibility measurements are explained on the basis of spin-glass-like behavior. Such behavior originates from competing FM and AFM interactions.

4. Conclusions

Polycrystalline samples of $Nd_{1-x}Ag_xMnO_3$ ($x = 0.05$, 0.10, 0.15 and 0.20) have been prepared for $x = 0$–0.20. All the samples are found to be in single-phase form. X-ray diffraction patterns could be refined by using the *Pbnm* space group. The lattice parameters a and c are found to increase with Ag doping. Temperature variation of magnetization measurement shows that these materials exhibit a paramagnetic–ferromagnetic transition with the signature of the presence of a competing antiferromagnetic transition. The paramagnetic susceptibility could be analyzed by using the Curie–Weiss law and the estimated μ_eff was comparable to the theoretical magnetic moments due to Mn^{3+}/Mn^{4+} and Nd^{3+} ions. The field variation of magnetization could be fitted to the Brillouin function relation by considering the FM interaction. The measured magnetization was explained on the basis of spin canting with a canting angle around 42°. The frequency variation of ac susceptibility and third harmonic susceptibility data indicate the presence of spin-glass-like behavior for $x = 0.10$ and 0.15 samples.

Acknowledgments

The authors are grateful to Dr Manoranjan Kar for useful discussions and Mr Bhaskar Roy Bardhan for his assistance in material preparation. The Department of Science and Technology, New Delhi is acknowledged for a research grant towards a magnetometer.

References

[1] Rao C N R and Raveau B 1998 *Colossal Magnetoresistance, Charge Ordering and Related Properties of Manganese Oxides* (Singapore: World Scientific)
[2] Ramirez A P 1997 *J. Phys.: Condens. Matter* **9** 8171
[3] Coey J M D 1999 *Adv. Phys.* **48** 167
[4] Tokura Y 2000 *Colossal Magneto-Resistive Oxides* (London: Gordon and Breach)
[5] Dagotto E, Hotta T and Moreo A 2001 *Phys. Rep.* **344** 1
[6] Salamon M B and Jaime M 2001 *Rev. Mod. Phys.* **73** 583
[7] Troyanchuk I O, Efimov D A, Samsonenko N V, Shapovalova E F and Szymczak H 1998 *J. Phys.: Condens. Matter* **10** 7957
[8] Liu K, Wu X W, Ahn K H, Sulchek T, Chien C L and Xiao J Q 1996 *Phys. Rev.* B **54** 3007
[9] Tokunaga M, Miura N, Tomioka Y and Tokura Y 1998 *Phys. Rev.* B **57** 5259
[10] Rao S S, Tripathi S, Pandey D and Bhat S V 2006 *Phys. Rev.* B **74** 144416

[11] Poddar A, Muruguraj P, Fischer R, Gmelin E, Bärner K, Haupt L, Mandal P and Rao G H 2004 *Physica* B **353** 324
[12] Pattabiraman M, Rangarajan G and Murugaraj P 2004 *Solid State Commun.* **132** 7
[13] Phan T L, Khiem N V, Phuc N X and Yu S C 2006 *J. Magn. Magn. Mater.* **304** e334
[14] Ritter C, Mahendiran R, Ibarra M R, Morellon L, Maignan A, Raveau B and Rao C N R 1999 *Phys. Rev.* B **61** R9229
[15] Srivastava C M, Dwivedi R K, Asthana S, Nigam A K and Bahadur D 2004 *J. Magn. Magn. Mater.* **284** 239
[16] Kajimoto R, Yoshizawa H, Kawano H, Kuwahara H, Tokura Y, Ohoyama K and Ohashi M 1999 *Phys. Rev.* B **60** R9506
[17] Caignaert V, Millange F, Hervieu M, Suard E and Raveau B 1996 *Solid State Commun.* **99** 173
[18] Li Z Q, Liu H, Cheng Y H, Mi W B, Yu A, Bai H L and Jiang E Y 2004 *Physica* B **353** 324
[19] Troyanchuk I O, Khalyavin D D, Trukhanov S V and Szymczak H 1999 *J. Phys.: Condens. Matter* **11** 8707
[20] Ryzhov V A, Lazuta A V, Khavronin V P, Larionov I I, Troaynchuk I O and Khalyavin D D 2004 *Solid State Commun.* **130** 803
[21] Gu B X, Zhang S Y, Zhang H C and Shen B G 1999 *J. Magn. Magn. Mater.* **204** 45
[22] Ghosh N, Elizabeth S, Bhat H L, Subanna G N and Sahana M 2003 *J. Magn. Magn. Mater.* **256** 286
[23] Jain H, Raychaudhuri A K, Ghosh N and Bhat H L 2007 *Phys. Rev.* B **76** 104408
[24] Liu X J, Jiang E Y, Li Z Q, Li B L, Li W R, Yu A and Bai H L 2004 *Physica* B **348** 146
[25] Li Z Q, Liu H, Liu X J, Liu X D, Bai H L, Sun C Q and Jiang E Y 2004 *J. Magn. Magn. Mater.* **284** 133
[26] Tang T, Tein C and Hou B Y 2008 *J. Alloys Compounds* **461** 42
[27] Tang T, Gu K M, Cao Q Q, Wang D H, Zhang S Y and Du Y W 2000 *J. Magn. Magn. Mater.* **222** 110
[28] Hien N T and Thuy N P 2002 *Physica* B **319** 168
[29] Pi L, Hervieu M, Maignan A, Martin C and Raveau B 2003 *Solid State Commun.* **126** 229
[30] Kar M and Ravi S 2004 *Mater. Sci. Eng.* B **110** 46
[31] Young R A 1996 *The Rietveld Method (International Union of Crystallography)* (New York: Oxford University Press)
[32] Wu S Y, Kuo C M, Wang H Y, Li W H, Lee K C, Lynn J W and Liu R S 2000 *J. Appl. Phys.* **87** 5822
[33] Muñoz A, Alonso J A, Lope M J M, Muñoz J L G and Fernández-Díaz M T 2000 *J. Phys.: Condens. Matter* **12** 1361
[34] Sudyoadsuk T, Suryanarayanan R and Winotai P 2004 *Solid State Commun.* **131** 681
[35] Srivastava S K, Kar M and Ravi S 2008 *J. Phys.: Condens. Matter* **20** 235201
[36] Srivastava S K, Kar M and Ravi S 2008 *J. Magn. Magn. Mater.* **320** e107
[37] Srivastava S K, Kar M and Ravi S 2006 *J. Magn. Magn. Mater.* **307** 318
[38] Cao G, Zhang J, Wang S, Yu J, Xu Y, Cao S, Jing C and Shen X 2000 *J. Magn. Magn. Mater.* **310** 777
[39] Gencer A, Ercan I and Özçelik B 1998 *J. Phys.: Condens. Matter* **10** 191
[40] Kouvel J S and Fischer M E 1964 *Phys. Rev.* A **136** 1626
[41] Tholence J L 1984 *Physica* B **126** 157 and reference cited therein
[42] Chakravarti A, Ranganathan R and Bansal C 1992 *Solid State Commun.* **82** 591
[43] Binder K and Young A P 1986 *Rev. Mod. Phys.* **58** 801
[44] Lévy L P 1988 *Phys. Rev.* B **38** 4963
[45] Ozcelik B, Kiymac K, Verstelle J C, Duyneveldt A J V and Mydosh J A 1992 *J. Phys.: Condens. Matter* **4** 5801
[46] Mathieu R, Asamitsu A, Kaneko Y, He J P and Tokura Y 2005 *Phys. Rev.* B **72** 14436